View Article Online
View Journal

Dalton Transactions

An international journal of inorganic chemistry

Accepted Manuscript

This article can be cited before page numbers have been issued, to do this please use: K. Bhardwaj, S. Pradhan, S. Basel, M. Clarke, B. Brito, S. Thapa, P. Roy, S. Borthakur, L. Saikia, A. Shankar, G. J. Stasiuk, A. Pariyar and S. Tamang, *Dalton Trans.*, 2020, DOI: 10.1039/D0DT02974B.

ROYAL SOCIETY OF CHEMISTRY

rsc.li/dalton

View Article Online
DOI: 10.1039/D0DT02974B

ARTICLE

Tunable NIR-II Emitting Silver Chalcogenide Quantum Dots using Thio/Selenourea Precursors: Preparation of MRI/NIR-II Multimodal Imaging Agent

Received 00th January 20xx,
Accepted 00th January 20xx

DOI: 10.1039/x0xx00000x

Karishma Bhardwaj,[a,‡] Sajan Pradhan,[a,‡] Siddhant Basel,[a] Mitchell Clarke,[b] Beatriz Brito,[b,c] Surakcha Thapa,[a] Pankaj Roy,[a] Sukanya Borthakur,[d] Lakshi Saikia,[d] Amit Shankar,[e] Graeme J. Stasiuk,[b,c,*] Anand Pariyar,[a] and Sudarsan Tamang[a,*]

Aqueous-stable, Cd- and Pb- free colloidal quantum dots with fluorescence properties in the second near-infrared region (NIR-II, 1000-1400) are highly desirable for non-invasive deep-tissue optical imaging and biosensing. The low band-gap semiconductor, silver chalcogenide offers a non-toxic and stable alternative to existing Pd, As, Hg and Cd-based NIR-II colloidal quantum dots (QDs). We report facile access to NIR-II emission windows with Ag_2X (X=S, Se) QDs using easy-to-prepare thio/selenourea precursors and their analogues. Aqueous phase transfer of these QDs with a high conservation of fluorescence quantum yield (retention up to ~90%) and colloidal stability is demonstrated. Bimodal NIR-II/MRI contrast agent with tunable fluorescence and high T_1 relaxivity 408 mM^{-1} s^{-1} per QD (size ~2.2 nm) and 990 mM^{-1} s^{-1} per QD (size ~ 4.2 nm) have been prepared by grafting 50 and 120 monoaqua Gd (III) complexes respectively to two different sized Ag_2S QDs. The size of the nanocrystals is crucial for tuning Gd payload and the relaxivity.

Introduction

In biological imaging, the second near-infrared (NIR-II, 1000-1400 nm) emitting fluorophores afford, in principle, a higher signal-to-noise ratio compared to their visible (400-750 nm) and the NIR-I (750-900 nm region) counterparts.[1–8] A combination of factors such as low absorbance of water and other biomolecules and low scattering/autofluorescence by tissue make the NIR-II window ideal for deep-tissue optical imaging and sensing with a high spatial and molecular resolution.[5–9] Compared to organic dyes, colloidal quantum dots (QDs) based NIR-II fluorophores have superior quantum yield, size-tunable fluorescence, broad absorption window and high molar extinction coefficient.[10–12] In addition, the surface of the QDs can be grafted with a high payload of functional molecules such as drugs, antibody, peptides, nucleic acids, cell-penetrating peptides, MRI contrast agent etc.[13–17] Specially, functionalizing QDs with another imaging agent such as a MRI contrast agent leads to the formation of a multimodal contrast agent which facilitates better visualization compared to a single imaging technique.[17–19] For example, MRI/NIR-II fluorescent imaging probes enable both excellent molecular level sensitivity (fluorescence) and anatomic resolution (MRI) due to the combination of fluorescence and MRI techniques. In recent years, the multimodal imaging agents have gained immense significance in the domain of biomedical imaging.[18–22]

The majority of the existing line of QDs -based NIR-II fluorophores contain highly toxic Cd^{2+}, As^{3-}, Pb^{2+} and Hg^{2+} ions[23,24] posing a real concern and practical barrier for their application in bio-imaging. In this respect, silver chalcogenides have tremendous potential in the field of *in vivo* bioimaging and sensing.[2–4,25–27] Ag_2S is non-toxic and has extremely low solubility product (K_{sp} = 6.3 × 10^{-50}) with minimum risk of releasing Ag^+ ions into the biological environment.[3,28,29] Furthermore, its low band-gap (bulk: 1.1 eV) and possible quantum confinement effect at size regime below 4 nm (exciton Bohr radius: 2.2 nm) are ideal for tuning of their emission in the ~700-1400 nm range.[13] Similarly, the bulk band-gap Ag_2Se is 0.15 eV[30,31] and their calculated exciton Bohr radius using bulk parameters is 2.9 nm. Strong absorption and emission tunability at sizes well below 4-5 nm are important for achieving low hydrodynamic diameter and renal-clearance from the body.[32] Studies have shown that Ag_2S exhibit negligible cytotoxic or genotoxic effects at lower to moderate doses, making it an ideal candidate for practical use in *in-vivo* imaging.[3,28,29,33,34] Despite tremendous potential in biology, the colloidal synthesis of Ag_2X (X=S, Se) is still less explored compared to II-IV, III-V and II-VI semiconductor NCs. Typically, the control of the size of Ag_2X QDs has been accomplished mainly either by changing of

[a] Department of Chemistry, School of Physical Sciences, Sikkim University, Sikkim 737102, India. E-mail: stamang@cus.ac.in
[b] Department of Biomedical Sciences, University of Hull, Hull, HU6 7RX, UK.
[c] Department of Imaging Chemistry and Biology, School of Biomedical Engineering and Imaging, King's College London, St Thomas' Hospital, London, SE1 7EH, United Kingdom. E-mail: graeme.stasiuk@kcl.ac.uk
[d] Department of Material Science, North East Institute of Science and Technology (NEIST), Assam 785006, India.
[e] Department of Physics, Kurseong College, West Bengal, India 734203.
‡ These authors contributed equally to this work.

Electronic Supplementary Information (ESI) available: NMR spectra, FTIR spectra, and TGA spectra of precursors. Additional optical characterization, photographs and XPS spectra of colloidal quantum dots solution. Optical constants of Ag_2S and DFT calculation. NMR, Mass and FTIR characterization of Gd complex and relaxivity studies data. See DOI: 10.1039/x0xx00000x

View Article Online
DOI: 10.1039/D0DT02974B

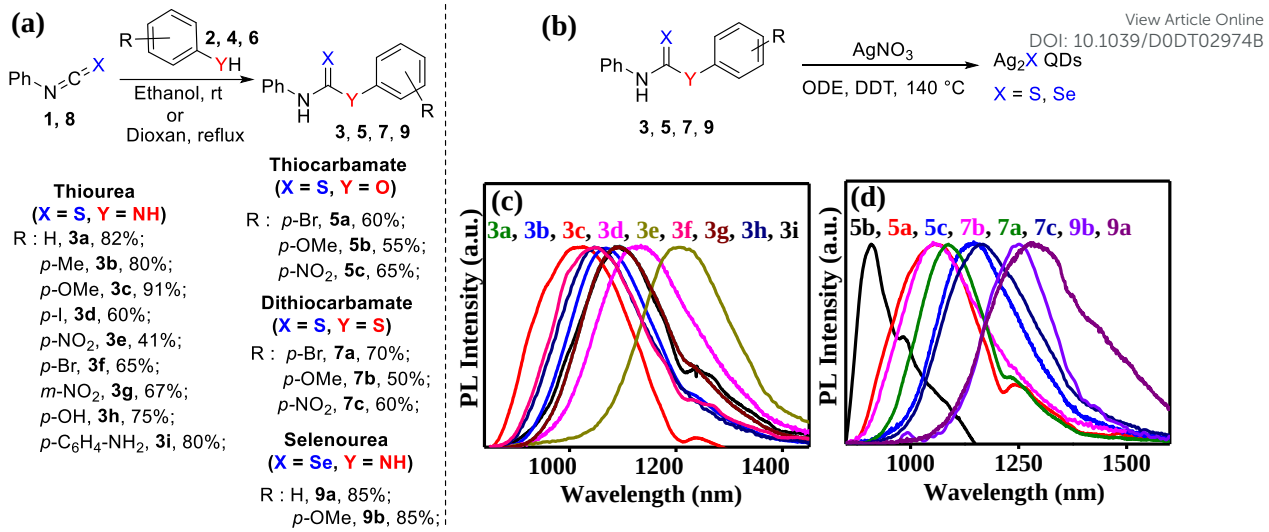

Figure 1. (a) Synthesis of a wide range of thiourea, thiocarbamate, dithiocarbamates and selenourea derivatives. (b) General scheme for the synthesis of Ag_2S/Se colloidal quantum dots (QDs). (c) PL spectra with tunable emission wavelength of as-prepared Ag_2S QDs synthesized from thiourea precursors (**3a-g**) and (d) Ag_2S/Se QDs synthesized from thiocarbamate (**5a-c**), dithiocarbamates (**7a-c**) and selenourea derivatives (**9a-b**).

temperature[35,36] and reaction time[31,37] or both the parameters.[38,39] Both changing time and temperature can lead to the tunability of average final size, however, the methods undermine the competitive effects such as Ostwald ripening and uncontrolled depletion of molecular precursor, both leading to diminished control over final size-distribution. Size-tunability of quantum dots is crucial in many important areas of bio-imaging including-but not limited to- (a) application in multiplexed identification of several bio-molecules as spectrally distinct barcodes,[40,41] (b) controlling hydrodynamic diameter for efficient clearance of the intravenously injected quantum dots from the body[32] and (c) controlling functional molecule pay-load in quantum dots-based multimodal contrast agents.[16,17,42]

A recent study by Vela *et al.* on II-VI semiconductor NCs[43,44] and Owen[45,46] *et al.* on the synthesis of II-VI and IV-VI semiconductor NCs have introduced a more rational approach to control the photophysical properties of nanocrystals (NCs) *via* the reactivity of precursor. Vela *et al.* demonstrated the impact of phosphine-chalcogenide precursor reactivity on the composition and morphology of CdS/CdSe NCs.[43,44] Similarly, the size-dependent optical properties of PbS/PbSe was later reported by Owen *et al.* by modulating the reactivity of thio/selenourea derivatives.[45,46] However, the strategies have so far not been extended to Ag_2X (X=S, Se) NCs. Herein, we report a facile synthesis of Ag_2X (X=S, Se) NCs with environmentally benign and biologically conducive attributes tunable in the crucial NIR region (900-1400 nm) by controlling the reactivity of substituted thio/selenourea and their analogues *via* modification of substituent groups. These NCs have been successfully phase transferred to the aqueous medium and functionalized with a T_1-weighed MRI contrast agent to prepare an MRI/NIR-II imaging agent. The details of the finding are in the following.

Result and discussion

We prepared a range of sulfur (substituted thiourea, thiocarbamate and dithiocarbamates) and selenium precursors with the direct reaction between isothiocyanate/isoselenocyanate with commercially available phenols, thiophenols or aryl amines (Figure1a). The reaction was carried out using off-the-shelf reagents in a suitable solvent such as chloroform, ethanol, dioxane or toluene at room temperature (*cf*. ESI; Experimental section), depending upon the solubility of the reactants. The reaction proceeds effortlessly yielding a good to excellent product yield (~up to 91 %) within a short time (~5-30 min, Figure 1a). In some cases, for example, in the reaction of nitro aniline with isothiocyanate in acetonitrile, heating to reflux temperature and longer reaction time is required. Inspired by the work of Owen and co-workers[46] on the synthesis of PbS, ZnS, SnS and CdS QDs using thiourea precursors, our initial attempt to synthesize the Ag_2S QDs by reacting Ag-oleate with thiourea in 1-octadecene (a non-coordinating solvent) at precursor decomposition temperature (~150 °C) was unsuccessful. No photoluminescence (PL) emission was detected and the colloidal dispersion was poor (Figure S2). The colloidal stability and optical properties could not be improved even when an amine (oleyl amine) was added during the reaction as a co-capping ligand (Figure S3). However, when 1-dodecanethiol (DDT) was used as a capping ligand, stable Ag_2S QDs was formed with excellent optical properties. DDT as capping ligand was found to be crucial for the successful synthesis of Ag_2S QDs as the soft acid Ag (I)ion prefers soft bases like thiol (-SH) or thiolate more than amines or carboxylates. We propose that the

View Article Online
DOI: 10.1039/D0DT02974B

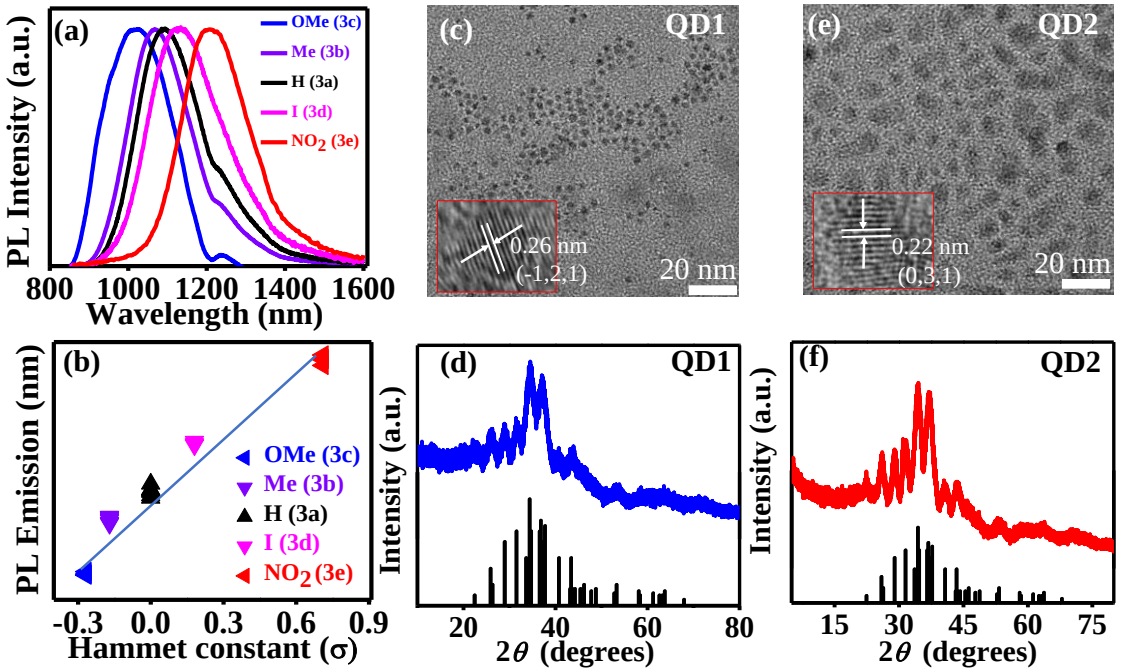

Figure 2. (a) PL spectra of Ag_2S QDs synthesized from thiourea precursors (**3a-e**) bearing various substituents at the para position of phenyl ring (H, *p*-Me, *p*-OMe, *p*-I and *p*-NO_2); (b) A linear correlation of PL emission wavelength (λ_{max}) obtained from (**3a-e**) with corresponding Hammett constants (σ) for *para* substituents. (c) TEM micrograph (size~2.2 ± 0.52 nm) and (d) XRD pattern of purified **QD1** obtained from **3c.** (e) TEM micrograph (size~4.2 ± 1.1 nm) of and (f) XRD pattern of purified **QD2** obtained from **3e.** Insets in figure c and e show the lattice fringes corresponding to the monoclinic phase. In figure d and f, the XRD reflections of monoclinic Ag_2S (JCPDS 14-0072) are shown as bars for comparison.

termination of surface of QDs with thiol-containing capping agents improve the colloidal stability and leads to monodisperse QDs with characteristic optical properties.[47–49] Furthermore, the standard redox potential of thiol-bound Ag^{1+} ion is lower than free Ag^{1+} ion which implies that the thiol-bound Ag (I) is not easily reduced to the undesired species.[31,47,48] In a typical synthesis of Ag_2S QDs, as prepared substituted thiourea (**3a-g**) dissolved in DME, was quickly injected to the hot solution of the silver precursor containing a mixture of $AgNO_3$ and DDT in ODE at elevated temperature (120-150 °C) (Figure 1b). A distinct color change from red to black after 15 min indicated the formation of Ag_2S QDs and the reaction was quenched by immediate cooling in an ice bath. To further understand the role of DDT we attempted to synthesize Ag_2S QDs using only DDT at the reaction temperatures (120-150 °C). No formation of Ag_2S QDs was noted in all the cases (Figure S4) possibly due to the high decomposition temperature (>170 °C) of DDT.[50] At elevated temperature (~200 °C) DDT formed Ag_2S QDs without the use of additional S precursor, as detected by XRD and optical studies (Figure S5). However, size distribution and optical properties (emission) were poor. On the contrary, the lower decomposition temperatures of as-prepared thiourea precursor (<150 °C) compared to DDT is conducive for controlled release of sulphur at the optimized reaction temperature (120-150 °C, Figure S6) leading to improved size distribution and optical properties. Fourier transform infrared spectroscopy (FTIR) experiment performed on purified Ag_2S QDs confirmed the presence of surface-bound DDT. The distinct shifting of the FTIR bands to 2916 cm^{-1} and 2847 cm^{-1} from 2922 cm^{-1} and 2851 cm^{-1} respectively attributed to the asymmetric and symmetric C-H stretching of DDT was observed (Figure S7).[51] These results show that DDT solely acts as the capping ligand for QDs in our synthetic scheme. Similarly, the other precursors such as thiocarbamates (**5a-c**) and dithiocarbamates (**7a-c**) as well as selenourea derivatives (**9a-b**) were also effective as a precursor under the optimized reaction condition to yield highly fluorescent Ag_2S/Se QDs. Figure 1c demonstrates the photoluminescence (PL) emission spectra of Ag_2S QDs in the NIR region (1020-1210 nm) prepared using (**3a-i**). Similarly, the NIR emission was also tunable in the range ~900 nm to 1300 nm by simply changing the substituent groups in thiocarbamates (**5a-c**), dithiocarbamates (**7a-c**) and selenourea precursors (**9a-b**) under optimized hot injection reaction condition (Figure 1d). In literature reports, the size of Ag_2X (X=S, Se) QDs has been controlled mainly by changing the reaction temperature[35,36] or the reaction time[31,37] or both the parameters.[38,39] Our results offer the opportunity to control the optical properties of Ag_2X (X=S, Se) QDs by controlling the precursor reactivity and conversion rates. In addition to this, the change of reaction temperature (Figure S8) and the reaction time (Figure S9) also affected the tunability of emission properties as

View Article Online
DOI: 10.1039/D0DT02974B

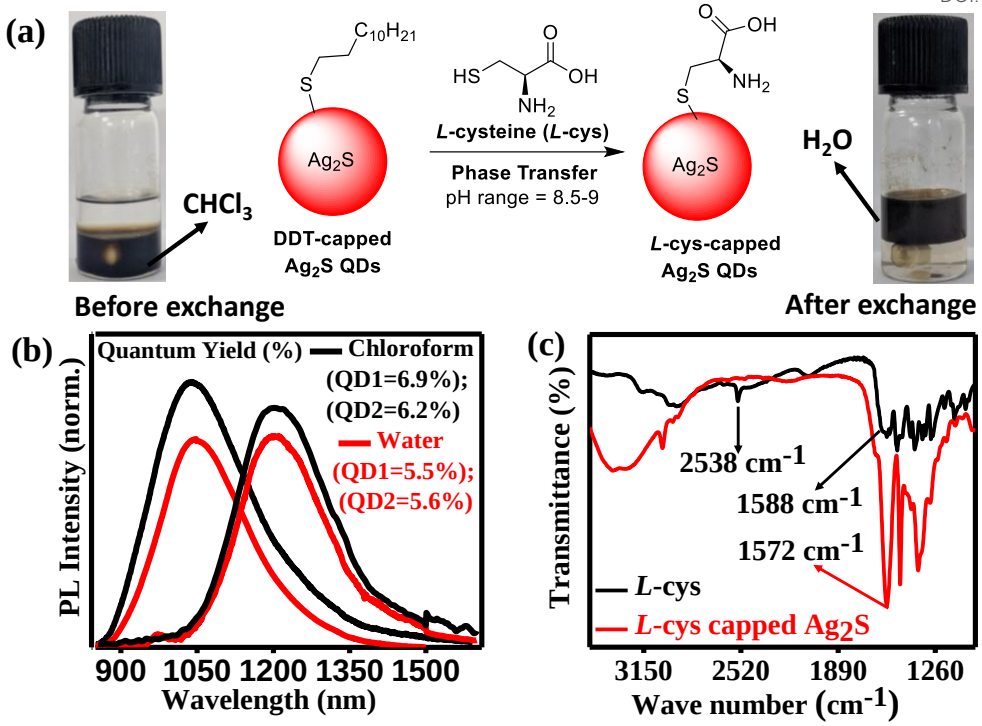

Figure 3. (a) Phase transfer of DDT-capped Ag_2S QDs from organic phase (chloroform) to aqueous phase using *L*-cysteine at pH ~9. (b) PL emission spectra of Ag_2S QDs (**QD1** and **QD2**) before (dispersed in $CHCl_3$, black) and after ligand exchange process with *L*-cysteine (dispersed in water, red). The spectra have been recorded at same absorbance (concentration) in both the phases. (c) FTIR spectra of free *L*-cysteine (black) and *L*-cysteine-capped Ag_2S QDs (red).

reported in the literature.

To understand the effect of thiourea conversion reactivity on the final size, Ag_2S QDs were synthesized using thiourea precursors (**3a-e**) with different substituent group under the same reaction condition (15 min, 150 °C). The final products were monitored using photoluminescence (PL) emission spectroscopy, X-ray diffraction (XRD) and transmission electron microscope (TEM) (Figure 2). The thiourea with no substituent group in the phenyl ring (**3a**) yielded Ag_2S QDs with a PL emission peak at 1094 nm (Figure 2a). On increasing the electron-donating ability by introducing methyl group as a *para* substituent in phenyl ring (*p*-Me, **3b**), the PL emission exhibited a distinct blue shift to 1071 nm. Further increasing the electron-donating ability by using *p*-OMe substituent in phenyl ring (**3c**) resulted in a blue shift in the PL emission (λ_{max}~1024 nm). In contrast, the presence of *p*-I substituent (**3d)** having moderate electron-withdrawing ability resulted in a red-shift of PL peak (λ_{max}~1133 nm). A significant red-shift (λ_{max}~1209 nm) was observed in the presence of **3e** bearing *p*-NO_2 group indicating the formation of larger sized Ag_2S QDs. Interestingly, the PL emission maxima linearly correlated with corresponding Hammett constant (σ) of the individual substituents (**3a-e**; H, *p*-Me, *p*-OMe, *p*-I and *p*-NO_2) of thiourea precursor corroborating a strong and predictable influence of electronic effects (Figure 2b).[52] Consistent with the PL spectra, the TEM images (Figure 2c, 2e) and XRD spectra (Figure 2d, 2f) confirm the difference in sizes of QDs formed using **3c** (**QD1**) and **3e** (**QD2**). Ag_2S QDs were fairly monodisperse with **QD1** and **QD2** of average sizes 2.2 ± 0.52 nm and 4.2 ± 1.1 nm respectively (Figure 2c and 2e). The XRD pattern for **QD1** was broader compared to that of **QD2** (Figure 2d and 2f) respectively due to the finite size effect and the diffraction patterns are consistent with monoclinic α-Ag_2S phase (JCPDS 14-0072).[53,54] The strong electron-withdrawing capacity of *p*-NO_2 group decreased the reactivity of the thiourea, leading to the formation of larger sized QDs compared. On the other hand, the presence of electron-donating group such as *p*-OMe led to enhanced reaction rate and smaller QDs. It is interesting to note that, this trend of size/emission tunability of Ag_2S QDs with respect to the reactivity of the substituted thiourea precursor is contrary to that observed in the case of PbS, ZnS or CdS QDs (Figure S10) in literature report[46] indicating that the underlining reaction pathway in our case is possibly different. A detailed investigation is required to map out the exact reaction mechanism, however, the above results can be explained by assuming rate-limiting nucleophilic attack on Ag^+ by the precursor through C=S bond. Furthermore, the electronics of other analogues of thiourea namely thiocarbamate (**5a-c**) and dithiocarbamates (**7a-c**) revealed a similar effect on the shift of PL of Ag_2S QDs. The thiocarbamate (**5b**) formed smaller Ag_2S QDs (λ_{max}~900 nm) due to its higher reactivity compared to thiourea and dithiocarbamates (Figure 1d). In the case of Ag_2Se QDs

View Article Online
DOI: 10.1039/D0DT02974B

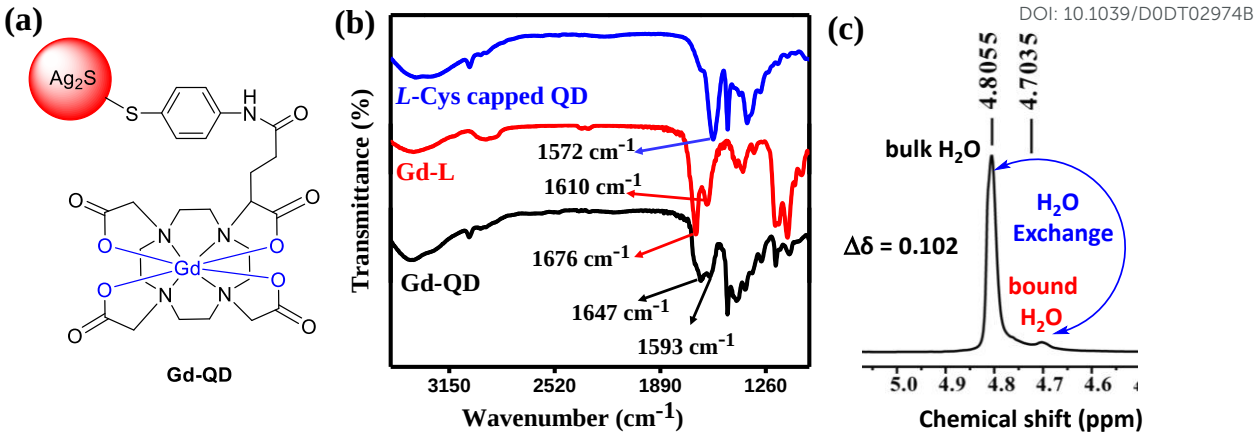

Figure 4. (a) Schematic representation of Gd^{3+} complex-capped Ag_2S QDs (**Gd-QD**) obtained by functionalization of *L*-cysteine-capped Ag_2S QDs with Gd^{3+} complex (**Gd-L**); (b) FTIR spectra of *L*-cysteine-capped Ag_2S QDs (blue), **Gd-L** (red) and **Gd-QD** (black); (c) ^{1}HNMR spectrum (400 MHz) of **Gd-QD1** demonstrating the exchange of water protons between bound and bulk water of surrounding.

synthesis, a similar trend in the shift of PL emission as a function of the para substituent (**9a** and **9b**) in selenourea derivative (Figure 1c and 1d) was observed. In some cases, such as **3i**, **5a** and **5b** (Figure 1c and 1d), small additional peak is observed in addition to the main PL emission, similar to that reported for silver chalcogenides and are attributed to the presence of surface defects.[30] Ag_2S and Ag_2Se NCs formed were further confirmed using X-ray photoelectron spectroscopy (XPS) (Figure S11 and S13). The C 1s signal was calibrated at 284.8 eV, prior to the assigning of other observed peaks (Figure S9a and S9b). Consistent with the literature report,[55,56] the presence of two prominent peaks at 368.9 eV and 374.9 eV in the Ag 3d core-level spectra of Ag_2S QDs (Figure S9c) are ascribed to Ag $3d_{5/2}$ and$3d_{3/2}$ respectively. The spectrum of S 2p (Figure S11d) could be deconvoluted to three individual components corresponding to S-H (162.9 and 164.1 eV), S-C (161.9 and 163.1 eV) and S-Ag (161.3 and 162.5 eV) as shown in the figure S12.[57] The individual peaks S2p1/2 and S2p3/2 corresponding to each component are separated by a spin–orbit splitting of ~1.2 eV[58] and have FWHM 1-1.2. The presence of S-C and S-H binding energies, in addition to S-Ag peak explain the observed atomic ratio (S/Ag) of 1.6: 1, which is on the higher side. This is attributed to the presence of the DDT on the surface of Ag_2S QDs which is also confirmed by FTIR results (Figure S7). Similar observation is also reported in the literature.[55]

The XPS spectra for Ag_2Se QDs are shown in Figure S13. These QDs have excellent colloidal stability in non-polar solvents such as hexane and toluene. However, the practical application of QDs for biomedical applications relies mostly on their colloidal stability in the aqueous system with the conservation of the optical properties.[59–62] In the following, we demonstrate the phase transfer and surface functionalization of the as-prepared QDs. We substituted hydrophobic surface ligands (DDT) with a hydrophilic ligand, *L*-cysteine in basic pH (Figure 3a). We chose *L*-cysteine due to its small size and zwitterionic nature, which are considered crucial for achieving compact size and low non-specific binding in the biological set-up.[61,62] The DDT-capped Ag_2S QDs of two different sizes **QD1** (size~2.2 nm) and **QD2** (size~4.2 nm) dispersed in chloroform showed a quantum yield (QY) of about 6.9 % and 6.2 % respectively (measured with respect to IR-140, the NIR-II standard dye as a reference, Figure 3b). The purified DDT-capped Ag_2S QDs dispersed in chloroform was subjected to ligand exchange process in the presence of *L*-cysteine dissolved in water at a pH~9 (*cf*. ESI; Experimental section).[62] The slightly elevated pH ensures deprotonation of thiol to thiolate. The pH of the phase transfer reaction is important because the metal-thiolate binding energy is higher than the metal-thiols.[62] The phase transfer was successful within 2 h yielding the *L*-cysteine-capped Ag_2S QDs in excellent yields (yield~93% and 90.0 % for **QD1** and **QD2** respectively) with a high conservation of the colloidal stability and the quantum yield (QY~5.5% and 5.6% for **QD1** and **QD2** respectively, Figure 3b). The FTIR spectrum of *L*-cysteine-capped Ag_2S QDs is depicted in Figure 3c. The FTIR spectrum of pure *L*-cysteine shows a characteristic S-H stretching vibration signal at 2538 cm^{-1} (Figure 3c). The absence of this peak in aqueous Ag_2S QDs (Figure 3c) confirmed the absence of unbound *L*-cysteine in solution. A prominent peak at 1572 cm^{-1} is ascribed to the asymmetric stretching vibration of carboxylate (COO^-) group of surface-bound *L*-cysteine. For free L-cysteine, this peak is observed at a slightly higher frequency (~1588 cm^{-1}).

Ag_2S QDs offer NIR-II emission with improved signal-to-noise ratio and functionalizing it with a T_1-weighed MRI contrast agent further improves its imaging efficiency and accuracy. We synthesized the Gd^{3+} based complex (**Gd-L**, Figure S14a) based on our earlier report[16] (*cf*. ESI; Experimental section) and subjected to the functionalization of the surface of *L*-

cysteine capped Ag_2S QDs to obtain an MRI/NIR-II fluorescence contrast agent, **Gd-QD** (figure 4a). We functionalized the surface of Ag_2S QDs of two different sizes **QD1** (Size~2.2 nm) and **QD2** (Size~4.2 nm) with **Gd-L** to obtain **Gd-QD1** and **Gd-QD2** respectively (*cf*. ESI; Experimental section). The Gd^{3+} based complex is known for its ability to lower the longitudinal relaxation *(T_1)* of bound water protons for improving localized signal intensity,[63] resulting in the enhancement of the image contrast.[64–73]

The FTIR spectrum of **Gd-L** complex (Figure 4b) showed peaks at 1676 cm^{-1} and 1610 cm^{-1} owing to the asymmetric stretching vibration of COO^- group and bending vibration of N-H group respectively. The successful grafting of Gd-L on to the Ag_2S QDs surface, thereby forming **Gd-QD** is confirmed by observation of asymmetric stretching vibration of COO^- group at a lower frequency (~1593 cm^{-1}). The broad absorption peaks at the range of 3000-3500 cm^{-1} are due to O-H and N-H stretching vibrations.[74] The formation of **Gd-QD** conjugate is further confirmed from nuclear magnetic resonance (NMR, 400 MHz) spectroscopy by monitoring the change in chemical shift of water due to the presence of the paramagnetic center. The difference in the chemical shifts of bulk and bound water (Δδ) for pure ligand, **Gd-L** is 0.3917 ppm (Figure S14b). After functionalization with **QD1** and **QD2**, the distinct change in Δδ was observed for both **Gd-QD1** (Δδ = 0.102, Figure 4c) and **Gd-QD2** (Δδ = 0.0301, Figure S14c) respectively. This result, taken together with FTIR result where no free **Gd-L** was detected, unanimously supports the successful grafting of Ag_2S with **Gd-L**. Notably, the smaller sized **Gd-QD1** exhibited a smaller longitudinal relaxivity (r_1) of 7.78 $mM^{-1}s^{-1}$ per **Gd-L** and *vice versa* was shown by larger sized **Gd-QD2** (r_1=8.27 $mM^{-1}s^{-1}$ per **Gd-L**). This is an increase from **Gd-L** which on its own exhibits an r_1 = 5.36 $mM^{-1}s$ (Figure S15 and S16). The higher relaxivity of **Gd-QD** compared to **Gd-L** is due to the presence of quantum dots which restricts free rotation in solution, therefore increasing r_1.[16] The concentration of Ag_2S QDs were determined at high photon energy (~450 nm), where molar extinction coefficient is independent of the size of QDs [75,76]. We used molar extinction coefficient of $1.73 \times 10^5\ M^{-1}\ cm^{-1}$ calculated using Ricard equation[77] at 450 nm (The optical constants used for calculation of molar extinction coefficient were determined using DFT, *cf*. ESI; Determination of Optical constants). At 400 MHz, the relaxivity per-QD for **Gd-QD1** and **Gd-QD2** was found to be 407.8 $mM^{-1}s^{-1}$ and 990.3 $mM^{-1}s^{-1}$ respectively (*cf*. ESI; Relaxivity measurements). Thus, the observed increase in relaxivity in **Gd-QD2** compared to **Gd-QD1** can be attributed to both the increase in the size of the nanocrystals which results in more restricted rotation in solution and increase in Gd payload due to larger surface area. In our study, we have demonstrated functionalization of the size-tunable Ag_2S QDs exhibiting fluorescence in biologically important NIR-II diagnostic window. The obtained values for relaxivity are much higher than the smaller complexes and the commercially available MRI contrast agents.[66] The comparison of longitudinal relaxivity values of **Gd-QD1**/**Gd-QD2** with other MRI contrast agents are listed in Table 1. The high longitudinal relaxivity values for both **Gd-QD1** and **Gd-QD2** in comparison to other nanoprobes suggest that **Gd-QD1** and **Gd-QD2** have a promising potential as a bright MRI contrast agent in bioimaging applications.

Table 1. Longitudinal relaxivity values of Gd-QD1/Gd-QD1 and other nanoprobes

nanoprobe	longitudinal relaxivity (*r*)
Gd-QD1	r_1 = 7.75 $mM^{-1}s^{-1}$
Gd-QD2	r_1 = 8.27 $mM^{-1}s^{-1}$
Gd-L	r_1 = 5.36 $mM^{-1}s^{-1}$
Gadovist[66]	r_1 = 4.34 $mM^{-1}s^{-1}$
Gd-doped QDs[67,74,78]	r_1 = 5.5–6.4 $mM^{-1}s^{-1}$
Gd_2O_3 nanoparticles[79]	r_1 = 6.9 $mM^{-1}s^{-1}$

Conclusions

A new method for the synthesis of bio-compatible silver chalcogenide QDs using easy-to-prepare substituted thiourea, thiocarbamate, dithiocarbamates and selenourea as S or Se precursors and DDT as capping agent is developed. The emission wavelength can be tuned in the NIR-II region by tuning reactivity of the precursor. The electronic effect of substituents groups and atoms on the size is evident from the blue or red shift in PL emission of the QDs consistent with electron-withdrawing or donating abilities of the substituent group. In the case of substituted phenyl containing precursors, the final size of QDs fits linearly with Hammett equation. The phase transfer of Ag_2S QDs from chloroform to aqueous phase was achieved by surface ligand exchange of DDT with *L*-cysteine and the aqueous QDs were subsequently functionalized with Gd^{3+} complex to form a dual-modal contrast agent with high NIR-II quantum yield (~5-6 %) and MRI T_1 water relaxivity (408-990 $mM^{-1}\ s^{-1}$ per QD) depending upon the size of the QDs.

Conflicts of interest

The authors declare no competing financial interest.

Acknowledgements

ST, SP and KB acknowledge SERB-DST, Government of India for research funding (EEQ/2016/000751 and EMR/2016/002505). SB would like to thank Department of Science and Technology, Government of India (DST/INSPIRE/03/2016/001207) [IF160689] for financial support under DST-INSPIRE Scheme. AP acknowledges SERB-DST (EEQ/2016/000685) and DST-Inspire (DST/INSPIRE/04/2015/002674), for financial assistance. ST and GJS thank the Royal Society (Grant IE160227) for finacial assistance. GJS would like to thank the Medical Reseasrch Council for funding (MR/T002573/1). AS acknowledges DST-

SERB (EEQ/2017/000319) for research funding. The authors thank Debesh Sharma, Khanindram Baruah and Sangeeta Saikia for initial help.

References

1 A. Zebibula, N. Alifu, L. Xia, C. Sun, X. Yu, D. Xue, L. Liu, G. Li and J. Qian, *Adv. Funct. Mater.*, 2018, **28**, 1703451.

2 G. Hong, J. T. Robinson, Y. Zhang, S. Diao, A. L. Antaris, Q. Wang and H. Dai, *Angew. Chem. Int. Ed.*, 2012, **51**, 9818–9821.

3 Y. Zhang, G. Hong, Y. Zhang, G. Chen, F. Li, H. Dai and Q. Wang, *ACS Nano*, 2012, **6**, 3695–3702.

4 Y. P. Gu, R. Cui, Z. L. Zhang, Z. X. Xie and D. W. Pang, *J. Am. Chem. Soc.*, 2012, **134**, 79–82.

5 K. Welsher, S. P. Sherlock and H. Dai, *Proc. Natl. Acad. Sci. U. S. A.*, 2011, **108**, 8943–8948.

6 J. T. Robinson, G. Hong, Y. Liang, B. Zhang, O. K. Yaghi and H. Dai, *J. Am. Chem. Soc.*, 2012, **134**, 10664–10669.

7 G. Hong, J. C. Lee, J. T. Robinson, U. Raaz, L. Xie, N. F. Huang, J. P. Cooke and H. Dai, *Nat. Med.*, 2012, **18**, 1841–1846.

8 Y. T. Lim, S. Kim, A. Nakayama, N. E. Stott, M. G. Bawendi and J. V. Frangioni, *Mol. Imaging*, 2003, **2**, 50–64.

9 A. M. Smith, M. C. Mancini and S. Nie, *Nat. Nanotechnol.*, 2009, **4**, 710–711.

10 S. Kim, Y. T. Lim, E. G. Soltesz, A. M. De Grand, J. Lee, A. Nakayama, J. A. Parker, T. Mihaljevic, R. G. Laurence, D. M. Dor, L. H. Cohn, M. G. Bawendi and J. V. Frangioni, *Nat. Biotechnol.*, 2004, **22**, 93–97.

11 J. Li and J. J. Zhu, *Analyst*, 2013, **138**, 2506–2515.

12 U. Resch-Genger, M. Grabolle, S. Cavaliere-Jaricot, R. Nitschke and T. Nann, *Nat. Methods*, 2008, **5**, 763–775.

13 S. J. Rosenthal, J. C. Chang, O. Kovtun, J. R. McBride and I. D. Tomlinson, *Chem. Biol.*, 2011, **18**, 10–24.

14 J. Zhou, Y. Yang and C. Y. Zhang, *Chem. Rev.*, 2015, **115**, 11669–11717.

15 G. Wang, Z. Li and N. Ma, *ACS Chem. Biol.*, 2018, **13**, 1705–1713.

16 G. J. Stasiuk, S. Tamang, D. Imbert, C. Poillot, M. Giardiello, C. Tisseyre, E. L. Barbier, P. H. Fries, M. De Waard, P. Reiss and M. Mazzanti, *ACS Nano*, 2011, **5**, 8193–8201.

17 H. Yang, S. Santra, G. A. Walter and P. H. Holloway, *Adv. Mater.*, 2006, **18**, 2890–2894.

18 L. E. Jennings and N. J. Long, *Chem. Commun.*, 2009, 3511–3524.

19 X. Michalet, F. F. Pinaud, L. A. Bentolila, J. M. Tsay, S. Doose, J. J. Li, G. Sundaresan, A. M. Wu, S. S. Gambhir and S. Weiss, *Science,* 2005, **307**, 538–544.

20 S. Lee and X. Chen, *Mol. Imaging*, 2009, **8**, 87–100.

21 Y. Jiao, Y. Sun, X. Tang, Q. Ren and W. Yang, *Small*, 2015, **11**, 1962–1974.

22 X. Gao, Y. Cui, R. M. Levenson, L. W. K. Chung and S. Nie, *Nat. Biotechnol.*, 2004, **22**, 969–976.

23 H. Sun, F. Zhang, H. Wei and B. Yang, *J. Mater. Chem. B*, 2013, **1**, 6485–6494.

24 P. Zrazhevskiy, M. Sena and X. Gao, *Chem. Soc. Rev.*, 2010, **39**, 4326–4354.

25 P. Jiang, C. N. Zhu, Z. L. Zhang, Z. Q. Tian and D. W. Pang, *Biomaterials*, 2012, **33**, 5130–5135.

26 G. Chen, F. Tian, Y. Zhang, Y. Zhang, C. Li and Q. Wang, *Adv. Funct. Mater.*, 2014, **24**, 2481–2488.

27 B. Dong, C. Li, G. Chen, Y. Zhang, Y. Zhang, M. Deng and Q. Wang, *Chem. Mater.*, 2013, **25**, 2503–2509.

28 D. He, S. Garg, Z. Wang, L. Li, H. Rong, X. Ma, G. Li, T. An and T. D. Waite, *Environ. Sci. Nano*, 2019, **6**, 1674–1687.

29 R. Gui, J. Sun, D. Liu, Y. Wang and H. Jin, *Dalt. Trans.*, 2014, **43**, 16690–16697.

30 M. Yarema, S. Pichler, M. Sytnyk, R. Seyrkammer, R. T. Lechner, G. Fritz-Popovski, D. Jarzab, K. Szendrei, R. Resel, O. Korovyanko, M. A. Loi, O. Paris, G. Hesser and W. Heiss, *ACS Nano*, 2011, **5**, 3758–3765.

31 C. N. Zhu, P. Jiang, Z. L. Zhang, D. L. Zhu, Z. Q. Tian and D. W. Pang, *ACS Appl. Mater. Interfaces*, 2013, **5**, 1186–1189.

32 H. Soo Choi, W. Liu, P. Misra, E. Tanaka, J. P. Zimmer, B. Itty Ipe, M. G. Bawendi and J. V. Frangioni, *Nat. Biotechnol.*, 2007, **25**, 1165–1170.

33 C. Lu, G. Chen, B. Yu and H. Cong, *Adv. Eng. Mater.*, 2018, **20**, 1700940.

34 P. Reiss, M. Carrière, C. Lincheneau, L. Vaure and S. Tamang, *Chem. Rev.*, 2016, **116**, 10731–10819.

35 I. Hocaoglu, M. N. Çizmeciyan, R. Erdem, C. Ozen, A. Kurt, A. Sennaroglu and H. Y. Acar, *J. Mater. Chem.*, 2012, **22**, 14674–14681.

36 Y. Zhang, Y. Liu, C. Li, X. Chen and Q. Wang, *J. Phys. Chem. C*, 2014, **118**, 4918–4923.

37 I. Hocaoglu, F. Demir, O. Birer, A. Kiraz, C. Sevrin, C. Grandfils and H. Yagci Acar, *Nanoscale*, 2014, **6**, 11921–11931.

38 P. Jiang, Z. Q. Tian, C. N. Zhu, Z. L. Zhang and D. W. Pang, *Chem. Mater.*, 2012, **24**, 3–5.

39 A. Sahu, L. Qi, M. S. Kang, D. Deng and D. J. Norris, *J. Am. Chem. Soc.*, 2011, **133**, 6509–6512.

40 M. Han, X. Gao, J. Z. Su and S. Nie, *Nat. Biotechnol.*, 2001, **19**, 631–635.

41 P. Zrazhevskiy, L. D. True and X. Gao, *Nat. Protoc.*, 2013, **8**, 1852–1869.

42 W. J. M. Mulder, R. Koole, R. J. Brandwijk, G. Storm, P. T. K. Chin, G. J. Strijkers, C. De Mello Donegá, K. Nicolay and A. W. Griffioen, *Nano Lett.*, 2006, **6**, 1–6.

43 Y. Guo, S. R. Alvarado, J. D. Barclay and J. Vela, *ACS Nano*, 2013, **7**, 3616–3626.

44 T. P. A. Ruberu, H. R. Albright, B. Callis, B. Ward, J. Cisneros, H. J. Fan and J. Vela, *ACS Nano*, 2012, **6**, 5348–5359.

45 M. P. Campos, M. P. Hendricks, A. N. Beecher, W. Walravens, R. A. Swain, G. T. Cleveland, Z. Hens, M. Y. Sfeir and J. S. Owen, *J. Am. Chem. Soc.*, 2017, **139**, 2296–2305.

46 M. P. Hendricks, M. P. Campos, G. T. Cleveland, I. J.-L. Plante and J. S. Owen, *Science,* 2015, **348**, 1226–1230.

47 P. Jiang and Z. Chen, *New J. Chem.*, 2017, **41**, 5707–5712.

48 L. Jing, S. V. Kershaw, Y. Li, X. Huang, Y. Li, A. L. Rogach and M. Gao, *Chem. Rev.*, 2016, **116**, 10623–10730.

49 A. Heuer-Jungemann, N. Feliu, I. Bakaimi, M. Hamaly, A. Alkilany, I. Chakraborty, A. Masood, M. F. Casula, A. Kostopoulou, E. Oh, K. Susumu, M. H. Stewart, I. L. Medintz, E. Stratakis, W. J. Parak and A. G. Kanaras, *Chem. Rev.*, 2019, **119**, 4819–4880.

50 L. Li and P. Reiss, *J. Am. Chem. Soc.*, 2008, **130**, 11588–11589.

51 J. Jayabharathi, G. A. Sundari, V. Thanikachalam, P. Jeeva and S. Panimozhi, *RSC Adv.*, 2017, **7**, 38923–38934.

52 E. J. Choi and S. B. Park, *Org. Biomol. Chem.*, 2015, **13**, 5202–5208.

53 Y. Du, B. Xu, T. Fu, M. Cai, F. Li, Y. Zhang and Q. Wang, *J. Am. Chem. Soc.*, 2010, **132**, 1470–1471.

54 S. I. Sadovnikov, A. I. Gusev, A. V. Chukin and A. A. Rempel, *Phys. Chem. Chem. Phys.*, 2016, **18**, 4617–4626.

55 J. Xiang, H. Cao, Q. Wu, S. Zhang, X. Zhang and A. A. R. Watt, *J. Phys. Chem. C*, 2008, **112**, 3580–3584.

56 Q. Wu, M. Zhou, J. Shi, Q. Li, M. Yang and Z. Zhang, *Anal. Chem.*, 2017, **89**, 6616–6623.

57 Q. Wu, M. Zhou, J. Shi, Q. Li, M. Yang and Z. Zhang, *Anal. Chem.*, 2017, **89**, 6616–6623.

58 J. Van Embden and Y. Tachibana, *J. Mater. Chem.*, 2012, **22**, 11466–11469.

59 L. Tan, A. Wan, T. Zhao, R. Huang and H. Li, *ACS Appl. Mater. Interfaces*, 2014, **6**, 6217−6222.

60 B. Dubertret, P. Skourides, D. J. Norris, V. Noireaux, A. H. Brivanlou and A. Libchaber, *Science,* 2012, **298**, 1759–1762.

61 W. Liu, H. S. Choi, J. P. Zimmer, E. Tanaka, J. V Frangioni and M. Bawendi, *J. Am. Chem. Soc.*, 2007, **129**, 14530–14531.

62 S. Tamang, G. Beaune, I. Texier and P. Reiss, *ACS Nano*, 2011, **5**, 9392–9402.

63 R. G. Aswathy, Y. Yoshida, T. Maekawa and D. S. Kumar, *Anal. Bioanal. Chem.*, 2010, **397**, 1417–1435.

64 S. G. McAdams, D. J. Lewis, P. D. McNaughter, E. A. Lewis, S. J. Haigh, P. O'Brien and F. Tuna, *Chem. Commun.*, 2017, **53**, 10500–10503.

65 V. S. Marangoni, O. Neumann, L. Henderson, C. C. Kaffes, H. Zhang, R. Zhang, S. Bishnoi, C. Ayala-Orozco, V. Zucolotto, J. A. Bankson, P. Nordlander and N. J. Halas, *Proc. Natl. Acad. Sci.*, 2017, **114**, 6960–6965.

66 P. Caravan, J. J. Ellison, T. J. McMurry and R. B. Lauffer, *Chem. Rev.*, 1999, **99**, 2293–2352.

67 X. Ren, L. Liu, Y. Li, Q. Dai, M. Zhang and X. Jing, *J. Mater. Chem. B*, 2014, **2**, 5541–5549.

68 G. J. Stasiuk, F. Minuzzi, M. Sae-Heng, C. Rivas, H. P. Juretschke, L. Piemonti, P. R. Allegrini, D. Laurent, A. R. Duckworth, A. Beeby, G. A. Rutter and N. J. Long, *Chem. Eur. J.*, 2015, **21**, 5023–5033.

69 N. A. Keasberry, M. Bañobre-López, C. Wood, G. J. Stasiuk, J. Gallo and N. J. Long, *Nanoscale*, 2015, **7**, 16119–16128.

View Article Online
DOI: 10.1039/D0DT02974B

70 C. Rivas, G. J. Stasiuk, M. Sae-Heng and N. J. Long, *Dalt. Trans.*, 2015, **44**, 4976–4985.

71 G. J. Stasiuk and N. J. Long, *Chem. Commun.*, 2013, **49**, 2732–2746.

72 N. G. Chabloz, M. N. Wenzel, H. L. Perry, I. C. Yoon, S. Molisso, G. J. Stasiuk, D. S. Elson, A. E. G. Cass and J. D. E. T. Wilton-Ely, *Chem. Eur. J.*, 2019, **25**, 10895–10906.

73 G. J. Stasiuk, S. Tamang, D. Imbert, C. Gateau, P. Reiss, P. Fries and M. Mazzanti, *Dalt. Trans.*, 2013, **42**, 8197–8200.

74 H. Chen, L. Wang, H. Fu, Z. Wang, Y. Xie, Z. Zhang and Y. Tang, *J. Mater. Chem. B*, 2016, **4**, 7472–7480.

75 S. Tamang, S. Lee, H. Choi and S. Jeong, *Chem. Mater.*, 2016, **28**, 8119–8122.

76 P. Yu, M. C. Beard, R. J. Ellingson, S. Fernere, C. Curtis, J. Drexler, F. Luiszer and A. J. Nozik, *J. Phys. Chem. B*, 2005, **109**, 7084–7087.

77 D. Ricard, M. Ghanassi and M. C. Schanne-Klein, *Opt. Commun.*, 1994, **108**, 311–318.

78 H. Chen, G. D. Wang, W. Tang, T. Todd, Z. Zhen, C. Tsang, K. Hekmatyar, T. Cowger, R. B. Hubbard, W. Zhang, J. Stickney, B. Shen and J. Xie, *Adv. Mater*, 2014, **26**, 6761–6766.

79 M. Ahrén, L. Selegård, F. Söderlind, M. Linares, J. Kauczor, P. Norman, P. Käll and K. Uvdal, *J. nanoparticle Res.*, 2012, **14**, 1–34.

View Article Online
DOI: 10.1039/D0DT02974B

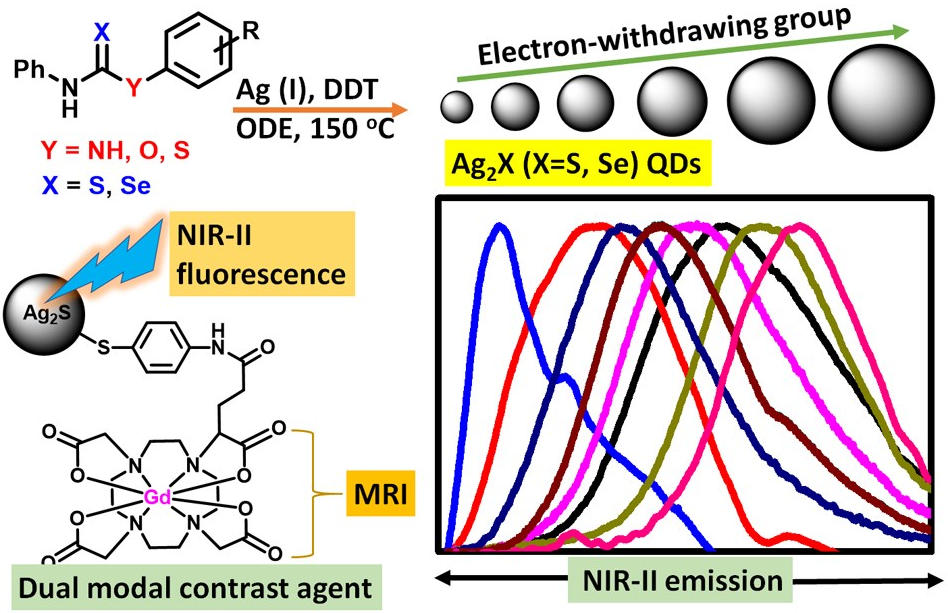

84x52mm (300 x 300 DPI)